

# Development of mechanical properties of concrete in vacuum tunnel of vacuum-based maglev train

Hongwei Lin<sup>a</sup>, Song Han<sup>a</sup>, Bing Han<sup>a,\*</sup>, Siming Liang<sup>b</sup>, Hailong Ye<sup>c</sup>, Haosu Liu<sup>d</sup>, Peng Feng<sup>e</sup>, Yalin Liu<sup>f</sup>, Guanzhi Cheng<sup>g</sup>

<sup>a</sup> School of Civil Engineering, Beijing Jiaotong University, Beijing 100044, China

<sup>b</sup> School of Civil Engineering, Sun Yat-sen University, Guangzhou 510275, China

<sup>c</sup> Department of Civil Engineering, The University of Hong Kong, Hong Kong, China

<sup>d</sup> Institute of Magnetic Levitation and Electromagnetic Propulsion, China Aerospace Science and Industry Corporation Limited, Beijing 100143, China

<sup>e</sup> Department of Civil Engineering, Tsinghua University, Beijing 100084, China

<sup>f</sup> National Center for Materials Service Safety, University of Science and Technology Beijing (USTB), Beijing 100083, China

<sup>g</sup> Railway Engineering Research Institute, China Academy of Railway Sciences Co., Ltd., Beijing 100081, China

## ARTICLE INFO

### Keywords:

Concrete  
Strength  
Elastic modulus  
Shrinkage  
Vacuum tunnel

## ABSTRACT

The vacuum-based maglev train is an emerging transportation system currently under development worldwide. While concrete is a technically viable material for constructing vacuum tunnels, its mechanical performance in this unique environment remains unclear. This paper investigates the behavior of concrete in vacuum using a large customized vacuum tube. The results show that concrete undergoes significant water loss in vacuum, resulting in impeded cement hydration and porous hydration products with a foam structure. Vacuum exposure during the early ages of concrete has negative effects on mechanical properties. However, once the cement hydration reaches a high level of maturity, further vacuum exposure has little influence. Compared with atmospheric conditions, the shrinkage of concrete in vacuum is significantly increased. These findings provide a valuable experimental database and new insights for the use of concrete in vacuum-based maglev trains.

## 1. Introduction

The transportation speed on land has been significantly increasing since the industrial revolution, which has greatly stimulated the prosperity of our human society. Currently, the fastest train in commercial use can reach a speed as high as 400 kilometers per hour. To further increase the speed, huge air resistance and noise are considered the bottleneck problems [1]. For this reason, researchers propose to combine high-speed trains with the vacuum tunnel, i.e., partly or completely removing the air surrounding the train. Countries including the United States, Switzerland, and Canada are all exploring this new transportation infrastructure system [2–6]. China is also devoting tremendous efforts to the ultra-high speed maglev train, which is a combination of magnetic propulsion and vacuum tunnel [7]. No full-scale hyperloop line was built until 2024, when a 2 km-test line of vacuum tunnel was constructed in Shanxi Province, China. Detailed discussions on the progress of this new transportation system can be found in [5]. In this cutting-edge transportation system, the sealed

tunnel with very thin air inside is the key infrastructure that enables the train to run at an ultra-high speed. Studies worldwide indicate that the concrete material is technically feasible for the construction of the vacuum tunnel [8–12]. However, the fundamental behaviors of concrete under vacuum environment remain largely unexplored and unclear.

The earliest studies on vacuum concrete date back to the 1980s under the background of lunar base construction. Cullingford et al. [13, 14] investigated the compressive strength, mass loss, and outgassing of concrete in vacuum. Their test results indicate that the compressive strength of concrete showed no degradation in vacuum ( $1.33 \times 10^{-2}$  Pa). In the 1990s, Powers-Couche and Lin [15] found that the fresh mortar in vacuum rapidly lost most of its water, and the hardened paste exhibited porous and friable characteristics, with little alteration in phase composition. Later, researchers in Japan carried out several studies in this respect. According to Horiguchi et al. [16], after 270 days of exposure in vacuum, the pores of  $0.2 \mu\text{m} \sim 7 \mu\text{m}$  of mortar reduced, while the pores of  $0.003 \mu\text{m} \sim 0.2 \mu\text{m}$  increased considerably. Similar conclusions were derived by Sakoi et al. [17], who found that the shrinkage

\* Corresponding author.

E-mail address: [bhan@bjtu.edu.cn](mailto:bhan@bjtu.edu.cn) (B. Han).

<https://doi.org/10.1016/j.conbuildmat.2024.137928>

Received 5 May 2024; Received in revised form 21 July 2024; Accepted 14 August 2024

Available online 22 August 2024

0950-0618/© 2024 Elsevier Ltd. All rights are reserved, including those for text and data mining, AI training, and similar technologies.

**Table 1**  
Chemical compositions of P·I 42.5 Portland cement (%).

SiO <sub>2</sub>	Al <sub>2</sub> O <sub>3</sub>	Fe <sub>2</sub> O <sub>3</sub>	CaO	MgO	SO <sub>3</sub>	Na <sub>2</sub> O <sub>eq</sub>	f-CaO	L.O.I	Cl <sup>-</sup>
20.60	4.57	3.29	63.27	2.59	2.11	0.55	0.76	2.15	0.026

**Table 2**  
Matrix of concrete specimens.

Label	Concrete	Environments	Number of specimens			
			Compressive strength		Tensile strength	Elastic modulus
			C	P	F	M
C30-*-A#		Atmosphere	27	27	27	27
C30-*-A1V#		1d in atmosphere, then vacuum	18	18	18	18
C30-*-A28V#	C30	28d in atmosphere, then vacuum	6	6	6	6
C30-*-A64V#		64d in atmosphere, then vacuum	9	-	-	-
C30-*-A76V#		76d in atmosphere, then vacuum	-	9	9	9
C50-*-A#		Atmosphere	15	15	15	15
C50-*-A3V#	C50	3d in atmosphere, then vacuum	15	15	15	15
C50-*-A28V#		28d in atmosphere, then vacuum	6	6	6	6

Note: “\*” represents the cubic compressive strength (C)/ prismatic compressive strength (P)/ flexural tensile strength (F)/ elastic modulus (M); the letter “A” represents the atmospheric environment, and the letter “V” represents the vacuum environment; “#” stands for the concrete age.



**Fig. 1.** Sealed tube for vacuum exposure.

of mortar in vacuum was two times larger than that in the atmospheric condition. They also found that the flexural and compressive strength of mortar increased with age even though there were some fluctuations. The tests by Hatanaka and Ishida [18,19] revealed that the early-age

hydration of ordinary Portland cement in vacuum was decelerated, and less hydration products and coarse pore structure were produced due to the rapid moisture evaporation. However, a different phenomenon was reported by Kanamori et al. [20]. In their tests, concrete specimens were pre-cured in water for 28 days and then moved to vacuum environment for one-year exposure. Test results revealed that concrete after vacuum exposure had larger compressive and flexural strength than those cured in water. Namba et al. [21] further pointed out that for concrete exposed to vacuum in the early stage, the vacuum exposure would have negative effects on its mechanical properties. The recent study by Pilehvar et al. [22] revealed that the vacuum could increase porosity and deteriorate compressive strength of 3D printed geopolymer concrete produced from lunar regolith simulant.

In recent years, Chinese researchers have renewed their interests in this field. Test results by Chang et al. [23] showed that the porosity of the cement stone exposed to vacuum were larger than those in atmosphere, while the compressive and flexural strength were smaller. However, Shangguan et al. [24] found that the vacuum exposure had positive effects on the compressive strength, but negative effects on the shear and flexural strength. The mechanism behind this abnormal phenomenon was elaborated by Shangguan et al. [24]. Their latest study further revealed that vacuum exposure could result in significant increase of drying shrinkage and water loss [25]. Targeting on the construction in plateau areas with elevation above 3000 m, some researchers in China investigated the effects of low air pressure on concrete properties [26–28]. They found that low air pressure could decrease cement hydration, increase porosity, and deteriorate the interfacial transition zone [29–33]. A systematic study on the effects of lower curing pressures on the microstructure formation of Portland cement pastes was conducted by Liu et al. [34]. In general, conclusions based on the low air pressure conditions are consistent with those found based on concrete in vacuum environment.

A summary of existing studies indicates that the vacuum exposure

**Table 3**  
Details of specimens for shrinkage tests.

Label	Concrete	Environment	Specimen size	Number of specimens
C30SH-A		Atmosphere		2
C30SH-A7V	C30	7d in atmosphere, then vacuum		2
C30SH-A14V		14d in atmosphere, then vacuum	400 mm×100 mm×100 mm	2
C30SH-A28V		28d in atmosphere, then vacuum		2
C50SH-A		C50		Atmosphere
C50SH-A28V	28d in atmosphere, then vacuum			1

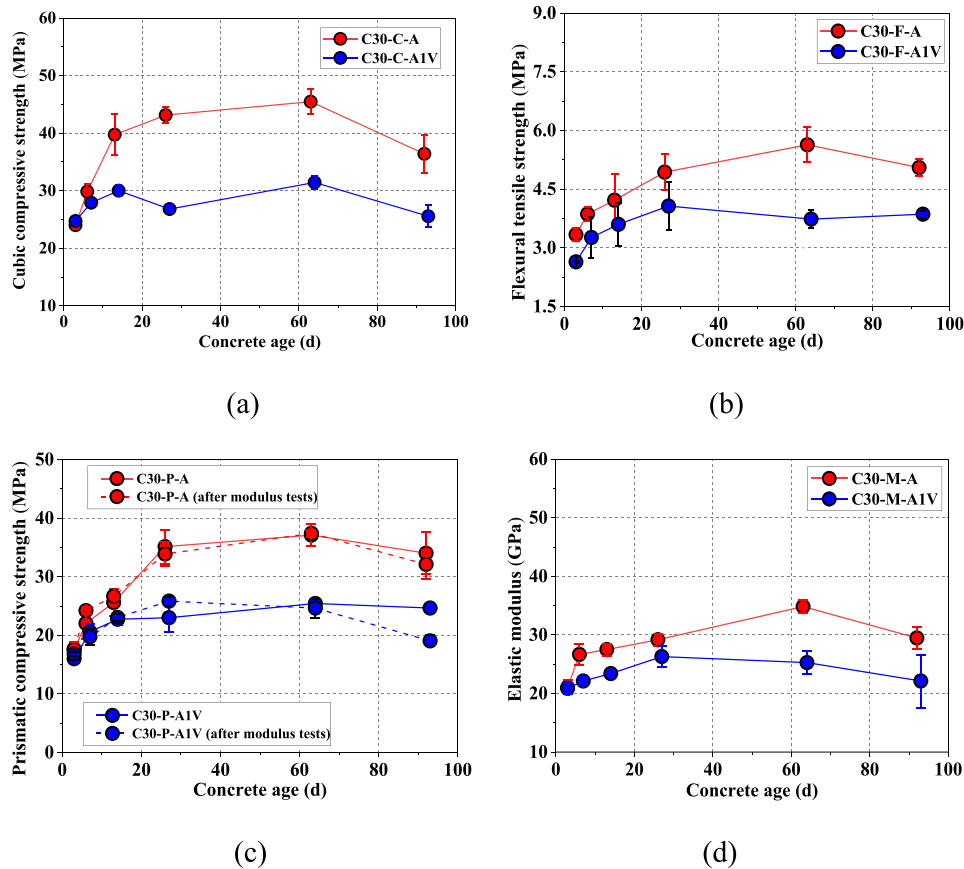


Fig. 2. Comparisons of mechanical properties of C30 concrete between atmospheric and vacuum specimens (C30-A1V).

will alter both the macroscopic behavior and microstructure of concrete. The adverse effects of vacuum exposure have been widely documented. Unfortunately, existing studies on concrete behavior in vacuum are far from enough. For instance, conflicting conclusions regarding the strength development and durability of concrete in vacuum can be found. To address those challenges, this paper provides a deep insight into the development of strength, elastic modulus, and shrinkage behavior of structural concrete based on a large number of experimental tests.

## 2. Experimental program

### 2.1. Mechanical tests

#### 2.1.1. Specimen fabrication

A 2 km-test line of vacuum tunnel for the ultra-high speed maglev train has been constructed by China Aerospace Science and Industry Corporation Limited in Shanxi Province. The concrete material used for this vacuum tunnel is C50 concrete. In view of this, C50 concrete was investigated in this study. Considering concrete with lower strength grade might be more sensitive to vacuum exposure and consequently the effects of vacuum exposure will be more pronounced, C30 concrete is also selected for comparison purpose. The investigation of C30 concrete in this study is not only helpful for understanding the effects of vacuum exposure on concrete behavior, but also enable researchers and engineers more choices in material selection for concrete structures in other vacuum environment.

The C50 specimens had a  $w/c$  of 0.4, and the corresponding mix proportion was: water: Portland cement: slag powder: fine aggregate: coarse aggregate = 320: 60: 893: 967: 3.8: 170 ( $\text{kg}/\text{m}^3$ ). This mix proportion is the same with that used for the 2 km-test line of vacuum

tunnel. The C50 specimens were produced in a local commercial concrete plant and P·O 42.5 Portland cement was used. According to the China standard [35], the P·O 42.5 Portland cement contains 5~20% supplementary cementitious materials (SCM). The manufactured sand with fineness modulus of 2.6 was used as fine aggregates, and the coarse aggregates were crushed limestone with a grain size of 5–16 mm. The aggregates all met the specified requirements of China standard [35]. The mixing water was the tap water. The C30 concrete specimens, which were fabricated in the laboratory, had a water-to-cement ( $w/c$ ) ratio of 0.55 and produced by using P·I 42.5 Portland cement. The chemical compositions of P·I 42.5 Portland cement are shown in Table 1. The relative mix proportion of all ingredients was as follows, water: Portland cement: fine aggregates: coarse aggregates = 230: 420: 665: 1085 ( $\text{kg}/\text{m}^3$ ).

In the construction of the 2 km-test line of vacuum tunnel, the concrete was cast and cured in atmosphere environment. The hardened concrete will stay in atmosphere environment for several months before vacuum exposure. To simulate this environment, concrete specimens cured in atmosphere for more than 28 days before vacuum exposure are designed. In order to get a better understanding on the effects of vacuum exposure on cement hydration, vacuum exposure of early age concrete (1 day and 3 day) is also considered. Table 2 shows the test environments of the concrete specimens. These specimens were first allowed to hydrate and harden in atmosphere for a designated period, followed by exposure to vacuum conditions. The examined mechanical properties of concrete included the cubic compressive strength, the prismatic compressive strength, the flexural tensile strength, and the elastic modulus. They were, respectively, measured on 100-mm cubes, 100 mm  $\times$  100 mm  $\times$  300 mm prisms, 100 mm  $\times$  100 mm  $\times$  400 mm prisms, and 100 mm  $\times$  100 mm  $\times$  300 mm prisms. In total, 384 specimens were manufactured, including 240 C30 specimens and 144 C50 specimens.

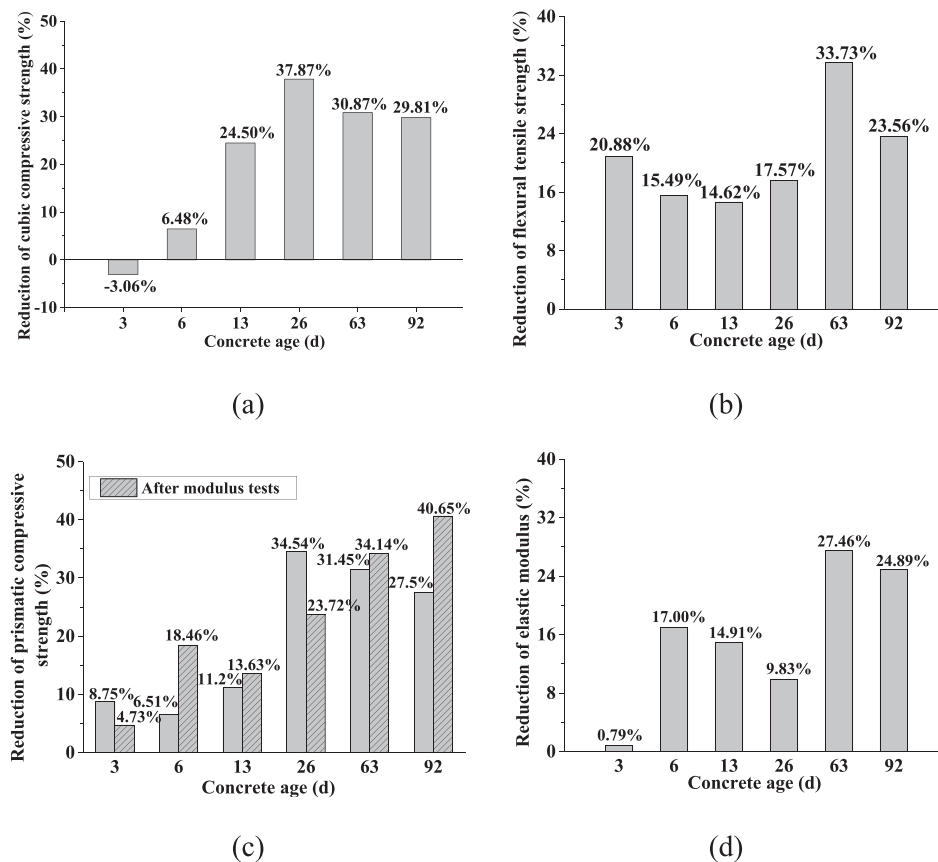


Fig. 3. Reduction of mechanical properties of C30 concrete exposed to vacuum at 1d.

For each specimen, there were 3 duplicates to counteract data scatter. Following the China standard [36], the concrete specimens were loaded by universal testing machines, with a loading rate of 0.3 MPa/s ~ 0.5 MPa/s. For strength testing, only the applied loads were monitored. After the elastic modulus tests, the specimens were further loaded to failure to obtain their compressive strengths. Therefore, there were 6 reference values for prismatic compressive strength at each combination of variables.

### 2.1.2. Equipment for vacuum environment

The equipment for creating the vacuum environment was designed and assembled by the Institute of Magnetic Levitation and Electromagnetic Propulsion of China Aerospace Science and Industry Corporation Limited. As shown in Fig. 1, the vacuum equipment was a circular steel tube with an outer diameter of 6.2 m and a length of 6 m. Inner the steel tube there is a C shape platform made of reinforced concrete. According to existing studies [2,5,23], the adopted air pressure in vacuum tunnel will be in the range of 0.1–0.001 atmosphere. Considering this, the air pressure in the vacuum tube was maintained around 2000 Pa during the tests.

Due to the inevitable outgassing of the tube, the air pressure inside the steel tube would slightly increase with time. To maintain a roughly constant pressure, timely evacuating was conducted. The temperature inside the sealed tube was not controlled during the tests. Test data by temperature sensors indicates that temperature inside the tube was the same as the temperature outside the tube, which was in the range of  $-10^{\circ}\text{C}\sim 36^{\circ}\text{C}$ .

## 2.2. Microstructure and morphology

According to the mix proportions of C30 and C50 concrete, two types of cement paste samples (excluding aggregates), i.e., CPI and CPII, were

prepared. The morphology of hydration products in hardened cement pastes under different environments was examined by Phenom Pharos G2 scanning electron microscopy (SEM) under an accelerating voltage of 15 kV. The freshly mixed cement pastes were cast into plastic tubes with a diameter of 25 mm. At the testing age, the hardened cement paste was segmented into discs with a thickness around 10 mm. For comparison purpose, each type of cement paste samples were divided into two groups: samples cured in the atmosphere and samples cured in the vacuum. For type CPI, the vacuum specimens were first cured in the standard curing room for 1 day before being vacuum exposure (CPI-A1V). For type CPII, the vacuum specimens were first cured in the standard curing room for 3 days or 28 days before vacuum exposure (CPII-A3V, CPII-28V). Prior to testing, samples were immersed in the isopropyl alcohol to arrest cement hydration [37]. The fractured surfaces of samples were sprayed with gold for SEM examination.

### 2.3. Pore structure characterization

The Mercury Intrusion Porosimetry (MIP) method was employed to evaluate the pore size distribution and porosity of hardened cement paste. The samples for MIP tests were the same with those in Section 2.2. They were broken into small pieces and tested on the AutoPore V 9620 at different curing ages. The applied pressure was in the range of 0.1 psi~61000 psi, and the testing range of pore diameter varies from 3.2 nm to 360  $\mu\text{m}$ .

### 2.4. Estimation of degree of hydration

Two methods were used to directly or indirectly analyze the degree of hydration (DoH) of hardened cement pastes, i.e., the BSE (back-scattered electron image) method and the TGA (Thermogravimetric analysis) method. The samples were the same with those in Section 2.2.

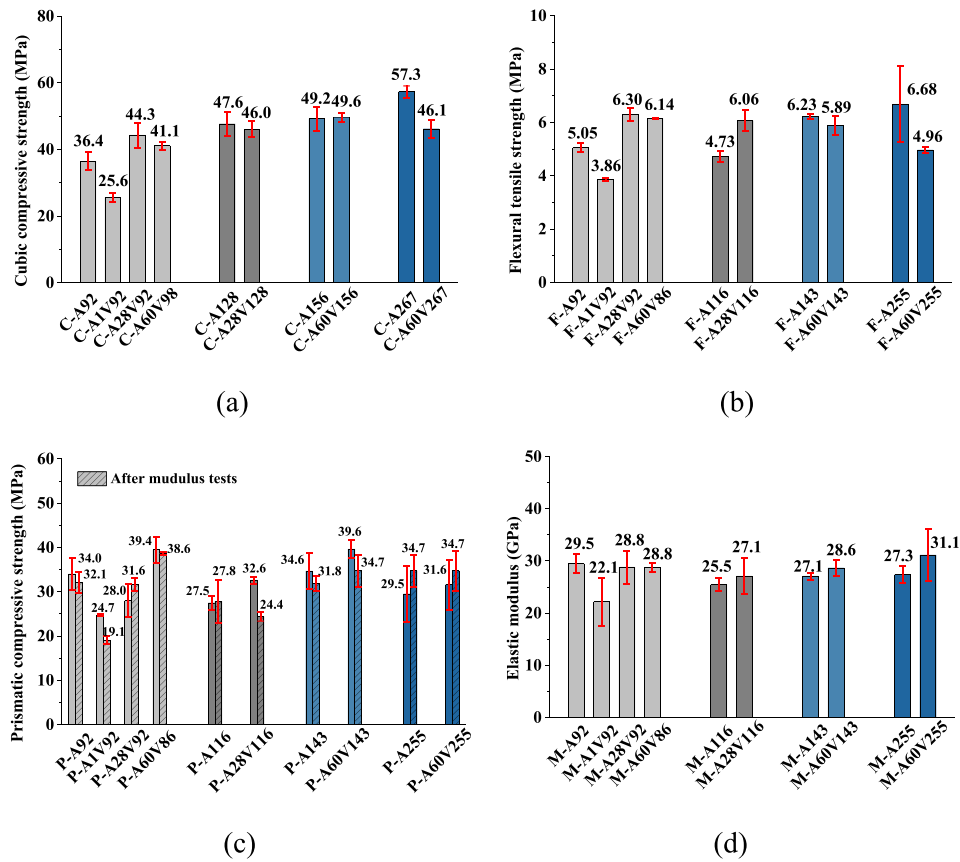


Fig. 4. Mechanical properties of C30 concrete in different environments.

The 10 mm-thick samples were embedded into the hardened epoxy resin and then subjected to polishing for a smooth and shiny surface. The BSE images were taken by Phenom Pharos G2. The images were magnified 1000 times with a resolution of 1920×1275, and the acceleration voltage was set to 15 kV. The working environment was low vacuum ranging from 0.1 Pa to 60 Pa. Samples from the same batch were maintained at the same contrast and brightness levels to ensure consistency in image grayscale. The microstructure and composition of cement-based materials were distinguished based on the grayscale characteristics of the BSE images, and the proportions of each phase can be determined by statistical analysis [38,39]. For each sample, 30 BSE images were randomly collected and analyzed using Image-Pro Plus software to calculate the volume content of cement clinker. Due to the presence of supplementary cementitious materials, it is inconclusive to accurately determine the degree of cement hydration. As a compromise, this paper estimates the degree of cement hydration by the relative volumetric proportion of unreacted binder including cement clinker and SCM.

The hydration degree of CPI samples was also analyzed by the thermogravimetric and derivative thermo-gravimetry (DTG) analysis (TG-DTG) method [40]. The TG-DTG analysis was conducted using a SETARAM thermogravimetric analyzer under a constant N<sub>2</sub> purging condition. Sample amounts of 50 mg were heated from 50 to 1000 °C at a fixed heating rate of 10 °C/min. The hydration degree can be calculated by the following equation [40],

$$\alpha_{bi} = \frac{W_{105^{\circ}C} - W_{1000^{\circ}C} - LOI}{nW_{1000^{\circ}C}} \quad (1)$$

where  $W_{105^{\circ}C}$  and  $W_{1000^{\circ}C}$  are the mass loss at 105 °C and 1000 °C respectively;  $n$  is the mass percent of non-evaporable water of fully hydrated cement,  $n = 0.25$  [40];  $LOI$  is the mass loss of P-I 42.5 Portland cement. The test data from the TG-DTG analysis was obtained under a

constant heating rate, and it is considered that most of the physically absorbed water had evaporated by 300 °C. Therefore, the mass loss at 300 °C was used instead of the mass loss at 105 °C.

### 2.5. Shrinkage tests

The shrinkage of concrete was measured based on 400 mm×100 mm × 100 mm prisms. Totally 10 specimens were fabricated, including 8 specimens made of C30 concrete and 2 specimens made of C50 concrete, as listed in Table 3. The shrinkage was measured by vibrating wire strain gauges [41]. The shrinkage and temperature in concrete were automatically recorded by automatic data acquisition system.

## 3. Results and discussions

### 3.1. Mechanical properties of concrete

#### 3.1.1. C30 concrete

Fig. 2 shows results of Series A and Series A1V of C30 specimens. With increasing age, concrete in both environments shows an overall increase in compressive strength, flexural tensile strength, and elastic modulus. For specimens in vacuum, the increase mainly takes place before 28 days, while for specimens in the atmosphere, the increase lasts until 60 days. The trend in vacuum is similar with that in the atmosphere, but vacuum exposure shows apparent negative effects on concrete properties. Fig. 3 shows the percentage of reduction of strength and elastic modulus. The reductions reach the peak between 28 and 60 days. At 90 days, it varies between 20 % and 40 %. Overall, the influence of the vacuum exposure on compressive strength, tensile strength, and elastic modulus is similar, and no significant differences are shown.

Fig. 4 presents results of all C30 specimens. At the age of 90 d, mechanical properties of concrete exposed to vacuum at 1 d (A1V) are the

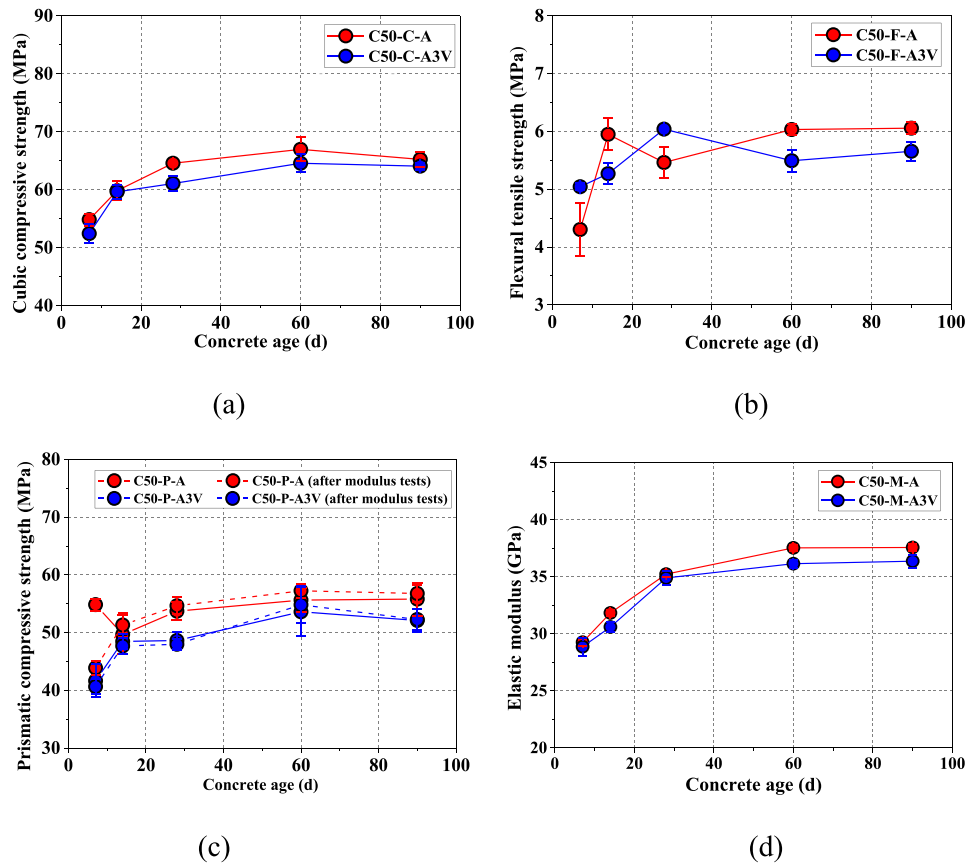


Fig. 5. Comparisons of mechanical properties of C50 concrete between atmospheric and vacuum specimens (C50-A3V).

lowest. For concrete exposed to vacuum at later ages (28 d or 60 d, Series A28V92, Series A60V98, Series A60V86), the tested strength and elastic modulus are comparable or even higher than those of atmospheric concrete. For instance, the compressive and tensile strength of specimens C-A60V98, F-A60V86 and P-A60V86 are 10~20 % larger than those of specimens in atmosphere. For specimens experienced longer vacuum exposure (Series A28V128, Series A28V116, Series A60V156, Series A60V143, Series A60V267, Series A60V255), this phenomenon still exists. In comparison with atmospheric concrete, 55.56 % of the specimens show an increase in compressive and tensile strength, and 100 % specimens show an increase in elastic modulus. The above observations reveal that vacuum exposure at early ages of concrete has adverse effects on the mechanical properties, however, vacuum exposure at later ages (e.g., later than 28 d) may be beneficial for strength and elastic modulus. The positive effects of vacuum exposure on concrete properties have also been reported by previous researchers, e.g., Kanamori et al. [20], Shangguan et al. [24]. An explanation for this phenomenon is that significant water evaporation of concrete in vacuum reduces the gaps between C-S-H gels, and consequently increases the surface energy. It has been confirmed by Chang et al. [23] that vacuum exposure significantly reduces the gel pores. As the cement matrix gets denser, the macro mechanical properties of concrete are hence improved.

### 3.1.2. C50 concrete

Similar to C30 concrete, the mechanical properties of C50 concrete in vacuum are inferior to those in the atmosphere (see Fig. 5). Fig. 6 shows the reduction of strength and elastic modulus. The reduction peaks at around 28 d~60 d. Compared with C30 concrete, the reduction of C50 concrete is less pronounced. At the age of 60 d, the cubic compressive strength, prismatic compressive strength, tensile strength, and elastic modulus in vacuum are respectively 3.58 %, 3.60 %, 8.96 %, and

4.27 % lower. This is because C50 concrete has a smaller  $w/c$  ratio, which will result in fast hydration reaction and denser internal structure. This can prevent the evaporation of free water in concrete in vacuum.

Fig. 7 shows test results of C50 concrete in different environments. Similar to C30 concrete, the specimens exposed to vacuum at early ages (Series A3V65, Series A3V98) have the lowest compressive and tensile strength, and elastic modulus. At the age of 65 d, the concrete which were in the atmosphere for 28 d before vacuum exposure have comparable mechanical properties with atmospheric concrete. However, at the age of 98 d, concrete which were in the atmosphere for 28 d before vacuum exposure have slightly larger strength and elastic modulus than atmospheric concrete. This supports the conclusion that the vacuum exposure at early ages is harmful for the development of mechanical properties, but vacuum exposure after 28 d has beneficial effects.

### 3.1.3. Relative mechanical properties

Knowledge on atmospheric concrete have been well established, therefore, they can be used as a reference for evaluating concrete in vacuum. The ratio of the strength or elastic modulus of concrete in vacuum to that of atmospheric concrete is defined as relative mechanical properties,  $R_{vac}$ . Fig. 8 shows the development of relative mechanical properties of concrete exposed to vacuum at early ages. In general, the relative values first increase with age and then decrease. At around 28 d~60 d, the relative strength or elastic modulus reaches the peak. Factors such as the  $w/c$  ratio, the concrete age of vacuum exposure, the pressure of vacuum environment, etc., can all influence the development of the relative mechanical properties. To evaluate the mechanical performance of concrete exposed to vacuum, the following empirical equation is proposed,

$$R_{vac} = 1 - m(e^{n(t-t_{vac})} - e^{2n(t-t_{vac})}) \quad (2)$$

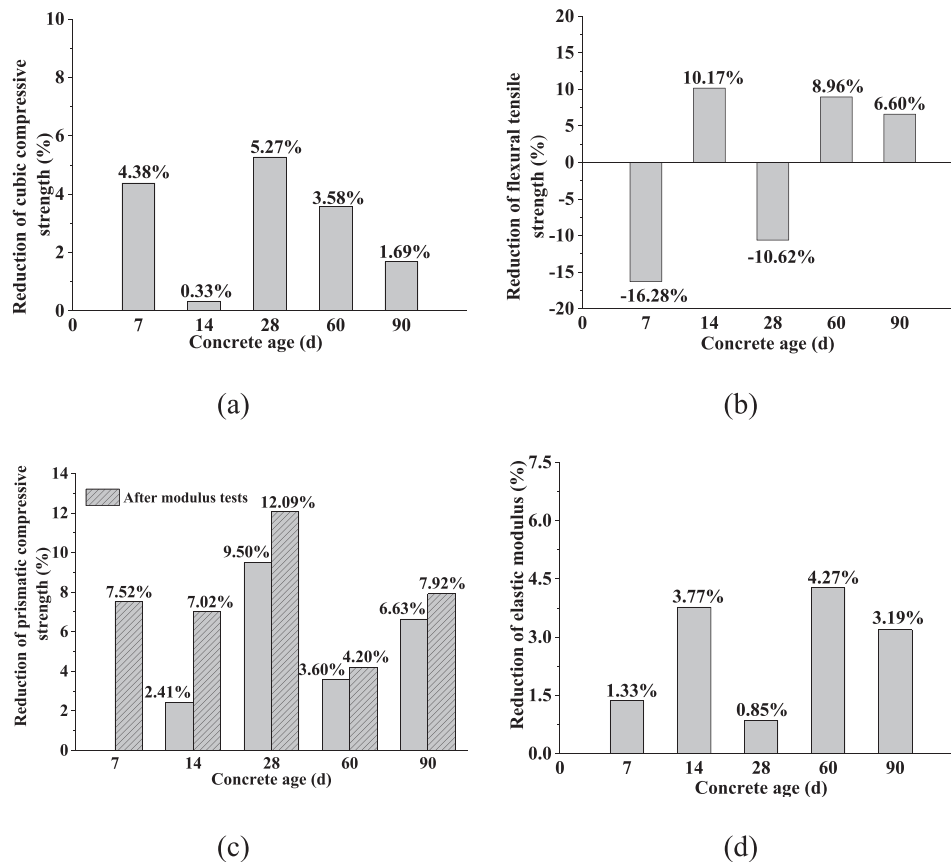


Fig. 6. Reduction of strength and elastic modulus of C50 concrete exposed to vacuum at 3d.

where  $t$  is the concrete age;  $t_{vac}$  is the concrete age initiating vacuum exposure;  $m$  and  $n$  are empirical parameters. Through regression analysis, the values of  $m$  and  $n$  are obtained (see Table 4). The average of the ratio of predicted to tested  $R_{vac}$  is 1.01 with a coefficient of variation (COV) of 8.6 %, as shown in Fig. 9. It is worth noting that the effectiveness of Eq. (2) should be further verified in the future due to the limited database in the current study. There are many factors influencing the development of strength and elastic modulus of concrete, such as the curing temperature, the humidity, et al. These parameters might be incorporated into Eq. (2) based on further studies.

### 3.2. Morphology of hydration products

Fig. 10 shows the morphology of 7-day CPI samples. In the SEM images, needles and flaky solids are visible. According to the morphology, it's inferred that the needles are ettringite, and the flakes are mainly C-S-H gels. In general, the micromorphology of hydration products generated in both environments are similar. However, more ettringite are observed in vacuum samples, and the C-S-H gels in vacuum are more porous. Fig. 11 presents the micromorphology of 28-day CPI samples. Most of the ettringite have disappeared, while C-S-H gels become dominant, which indicates an increased degree of cement hydration for samples in both environments. Compared with samples in atmosphere, samples in vacuum show a much more porous foam-like structure, as characterized by pores with a diameter of less than 1  $\mu\text{m}$ . At 80000x magnification, the foam structure is more distinguishable, as shown in Fig. 12. The probable reason is that in vacuum, free water that has not yet participated in the hydration reaction evaporates. Because the internal pressure is greater than the external pressure, water vapor (including air and water) diffuses from the inside of the sample to the outside, with the volume continuously expanding, leaving a foamy structure in the cement paste that has not yet fully hardened.

Fig. 13 shows the micromorphology of 28-day CPII samples. The microstructure of hydrated products generated in vacuum and atmospheric environment is visibly different. In the atmosphere, the C-S-H gels appear relatively dense, whereas in vacuum, they exhibit a porous or net-like structure, accompanied by needle-shaped ettringite, which is consistent with that of CPI samples. However, the foam structure of CPII samples is less pronounced. This is because CPII samples were exposed to vacuum after 3 days of curing in atmospheric environment, during which the degree of hydration was relatively high. Additionally, the  $w/c$  ratio of CPII samples was smaller, making the internal structure denser than that of CPI samples, which reduced the water evaporation. Both factors contributed to mitigating the negative effects of vacuum exposure.

Fig. 14 illustrates the micromorphology of 150-day CPII samples under varying environmental conditions. It is evident from the SEM images that the microstructure of the hydration products (mainly C-S-H gels) of A3V150 samples has obvious vesicular or foam structures, which is similar to samples of 28 d age (A3V28). This indicates that the foam structure will not disappear with increasing concrete age. The microstructure of the hydration products of A150 samples and the A28V150 samples appear relatively dense without significant differences. This suggests that vacuum exposure will not significantly impact the microstructure of the hydration products if the cement paste has almost fully hardened in atmospheric environment.

### 3.3. Degree of cement hydration

#### 3.3.1. BSE results

Fig. 15 shows backscattered electron (BSE) images of CPI and CPII samples. For the CPI specimens, the phases in the BSE images can be roughly classified into four categories based on their grayscale values from high to low: pores and cracks, hydrated C-S-H and hydrated

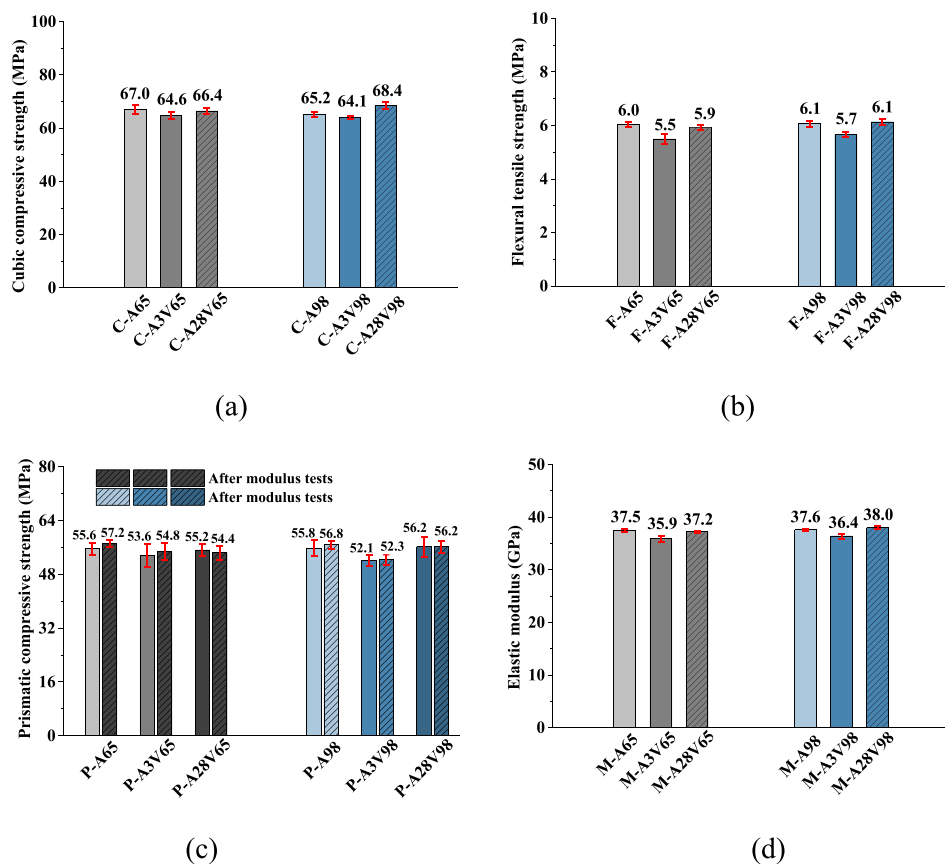


Fig. 7. Mechanical properties of C50 concrete in different environments.

(sulfate) aluminate, calcium hydroxide (CH), and unhydrated cement clinker. The CPI samples in vacuum have relatively few hydration products, and many interconnected pores can be observed between the hydration products. In contrast, the CPII specimens show many phases with clear boundaries and grayscale values lower than those of the cement hydration products. Grayscale and morphology characteristics reveal that this phase is unreacted supplementary cementitious material (SCM) [42,43].

Fig. 16 shows the percentage of cement clinker in CPI and CPII samples. In CPI samples, the proportion of cement clinker in vacuum samples is higher than in atmospheric samples (Fig. 16a), suggesting that cement in vacuum is less hydrated than that in the atmosphere. With the increase of concrete age, the proportion of cement clinker decreases in both environments. Notably, the degree of hydration in vacuum specimens at 28 days does not reach that of 7-day specimens in atmospheric environment. Similar conclusions can also be drawn for CPII specimens (see Fig. 16b). However, for CPII-A28V150 samples, the percentage of cement clinker is even lower than that of atmospheric samples (CPII-A150). There are two possible reasons for this unusual phenomenon: firstly, the long-term vacuum exposure resulted in absolute dryness of the samples, making the cement clinker easily ground off during sample polishing; Secondly, during the 150-day vacuum exposure, the vacuum tube underwent several cycles between the atmospheric pressure and low vacuum, leading to gas exchange between concrete pores and the outside environment. The high-flow gas brought the cement clinker to the outside environment. The authors tested the dust collected from the vacuum tube, and found the cement clinker originated from the inner matrix of concrete. Through a series of tests, the authors have confirmed the aerodynamic damage of concrete due to alternating air pressure cycles [44].

BSE images of CPII samples also reveal the presence of numerous micro-cracks in vacuum environment (see Fig. 17). The continuous lines

in the figure are cracks automatically identified by the software. The CPII-A3V150 sample exhibits the most cracks, followed by the CPII-A28V150 sample, while the samples cured in atmospheric environment showed significantly fewer micro-cracks. This is because in vacuum environment, the free water in the cement paste evaporates extensively, causing the matrix to shrink and crack. The earlier the samples were exposed to vacuum, the lower the matrix strength and the more water evaporates. According to Zhang et al. [45], a higher evaporation rate results in larger drying shrinkage. A recent study by Yin et al. [46] indicates that the shrinkage due to fierce drying conditions is accompanied by the collapse of a large amount of collapsible gel pores (2.6–50 nm), which may cause severe cracking of matrix. Thus, earlier vacuum exposure makes the matrix more susceptible to shrinkage cracking.

### 3.3.2. TG-DTG results

Fig. 18 shows the TG-DTG curves of CPI specimens. As can be seen, the weight loss of the samples under vacuum and atmospheric environments is similar. The sample shows significant weight loss at 400–550°C [47–49], corresponding to the decomposition of portlandite. At 7 days of age, the content of portlandite produced in vacuum is slightly lower than that of atmospheric cement paste, and at 28 days of age, the difference enlarges. Portlandite is a part of the hydration products, and a higher content of portlandite indicates a higher degree of cement hydration.

According to Eq. (1), the degree of hydration of CPI samples can be obtained, as shown in Fig. 19. At 7 d and 28 d ages, the DoH of cement pastes in vacuum is apparently lower than that of samples in the atmospheric environment. With the increase of age, increase of DoH of cement pastes in both environments can be observed, however, samples in vacuum show limited increase compared with atmospheric samples. In fact, the DoH of cement pastes in vacuum at 28 d age is even lower

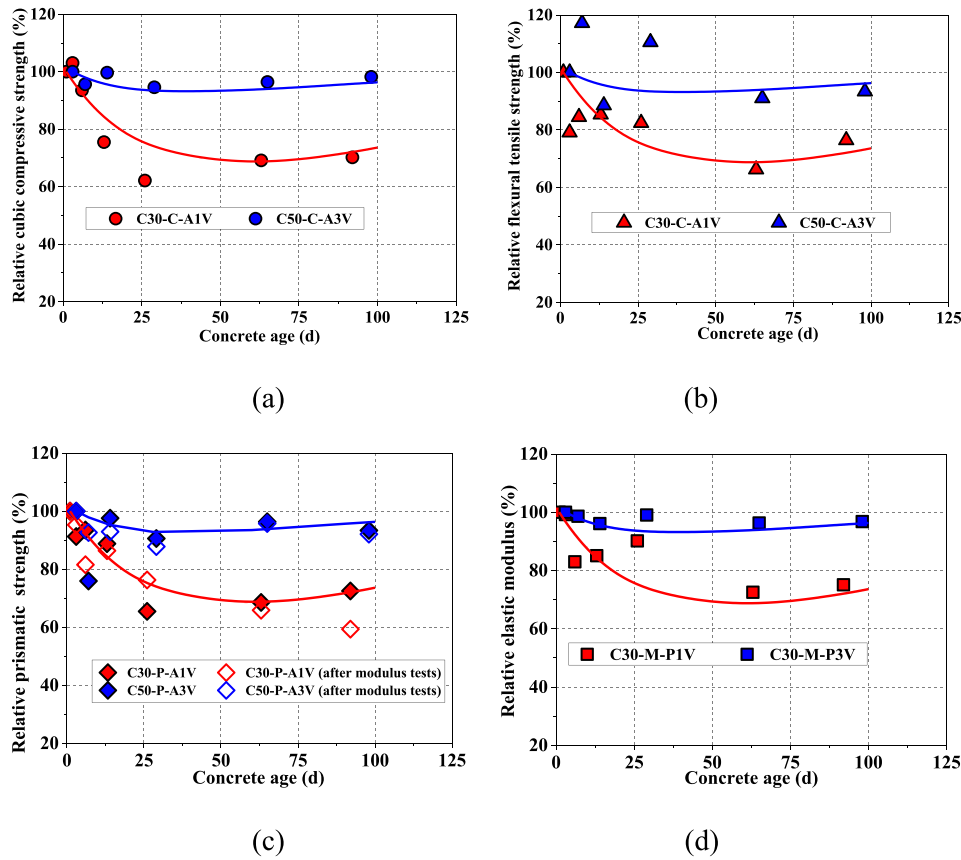


Fig. 8. Relative mechanical performance of concrete exposed to vacuum at early ages.

Table 4  
Regressed values of parameter  $m$  and  $n$ .

Empirical parameters	C30 concrete			C50 concrete	
	$t_{vac}=1$	$t_{vac}=28$	$t_{vac}=60$	$t_{vac}=3$	$t_{vac}=28$
$m$	1.32	-0.27	-0.34	0.3	0.02
$n$	-0.013			-0.02	

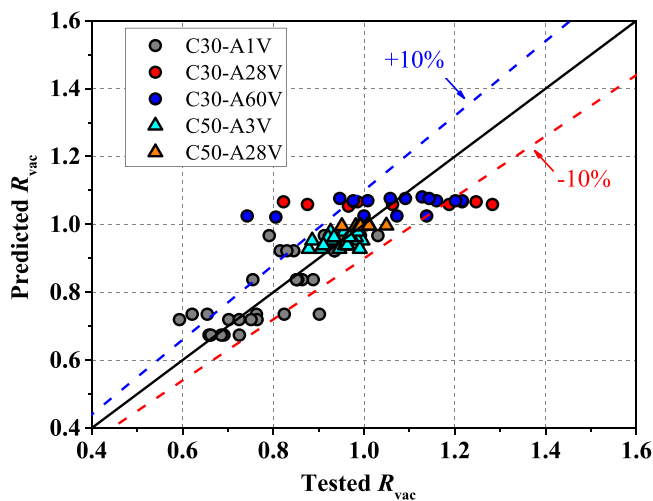


Fig. 9. Comparisons of predicted and tested  $R_{vac}$ .

than that of cement pastes in the atmospheric environment at 7 d age. This clearly demonstrates the negative effect of vacuum exposure on cement hydration.

### 3.4. Pore structure

Fig. 20 shows the MIP pore size distribution of CPI samples. The pore size distribution of specimens in both environments is similar. However, the porosity of vacuum specimens is much higher, and the difference enlarges with increasing age. Compared with atmospheric specimens, the number of harmless pores (the diameter  $R < 20$  nm) and less harmful pores ( $20 \text{ nm} < R < 100$  nm) decreases in vacuum specimens, while the number of harmful pores ( $100 \text{ nm} < R < 200$  nm) and highly harmful pores ( $R > 200$  nm) around 1000 nm significantly increases. Fig. 21 shows the total porosity, mean pore size, and characteristic pore size. Compared with atmospheric specimens, the total porosity of vacuum specimens increases by 3.43 % and 9.23 % at the age of 7 days and 28 days, the mean pore size increases by 38.74 % and 99.33 %, and the characteristic pore size increases by 55.02 % and 23.24 %, respectively. It can also be noted that the total porosity of specimens in both environments decreases with age, while the mean pore size increases. This is due to that the hydration products of cement fill the original free water space.

Fig. 22 shows the MIP pore size distribution of CPII specimens. While samples in different environments exhibit similar pore structure, A3V samples have the highest porosity and a reduction in capillary pores around 10 nm in diameter, whereas pores around 100 nm have increased significantly. Notably, the pore size distribution of A28V150, which was exposed to vacuum at 28 d age, is comparable to that of atmospheric samples A150. These results suggest that vacuum exposure of concrete at early ages coarsens the pore structure, but vacuum exposure at later ages, for instance, later than 28 d, has limited influence on the

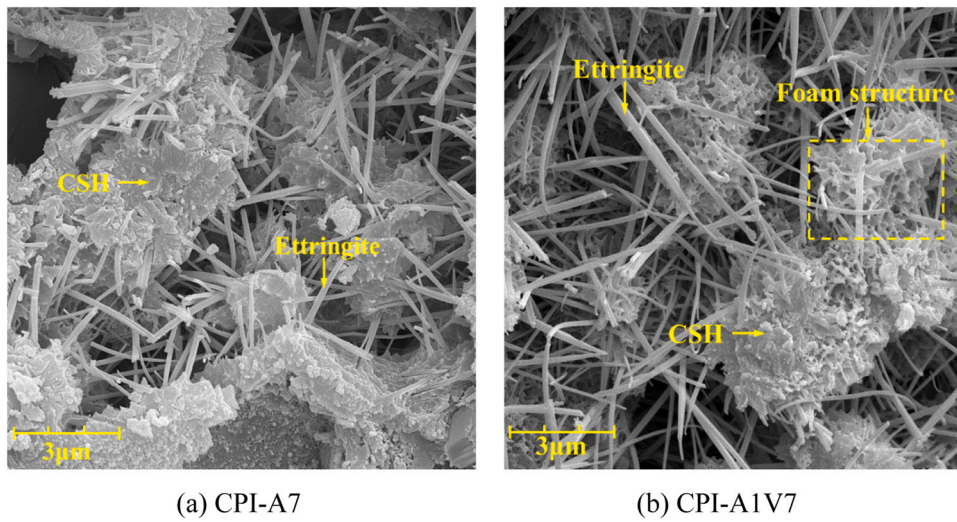


Fig. 10. SEM images of CPI samples at 7d age (20000x).

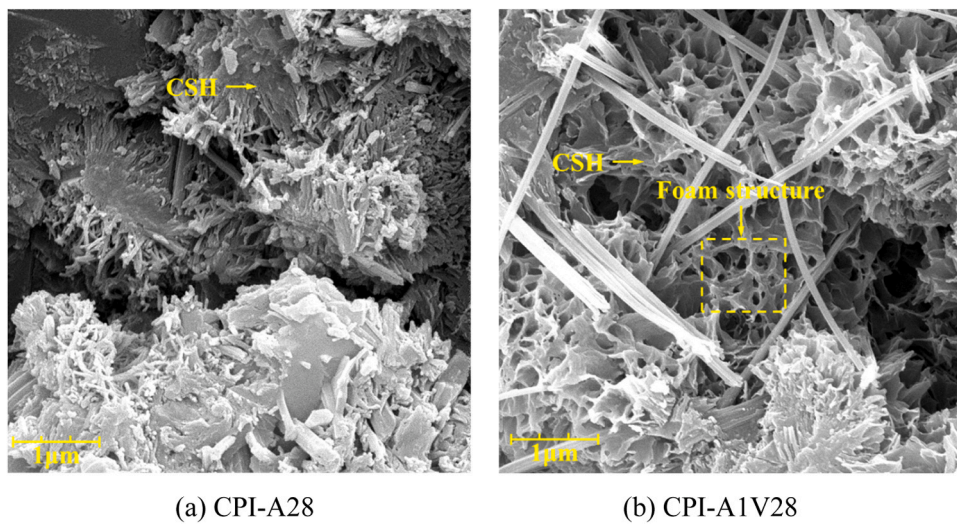


Fig. 11. SEM images of CPI samples at 28d age (50000x).

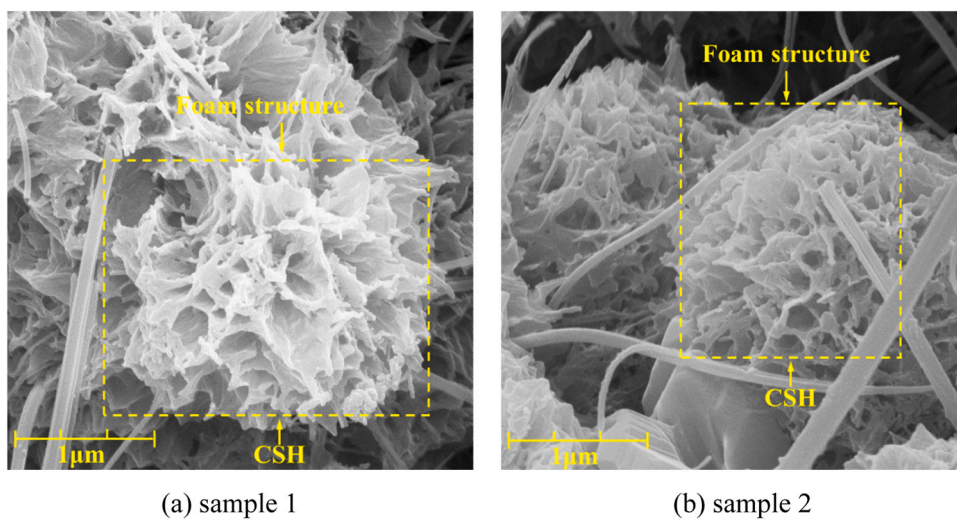
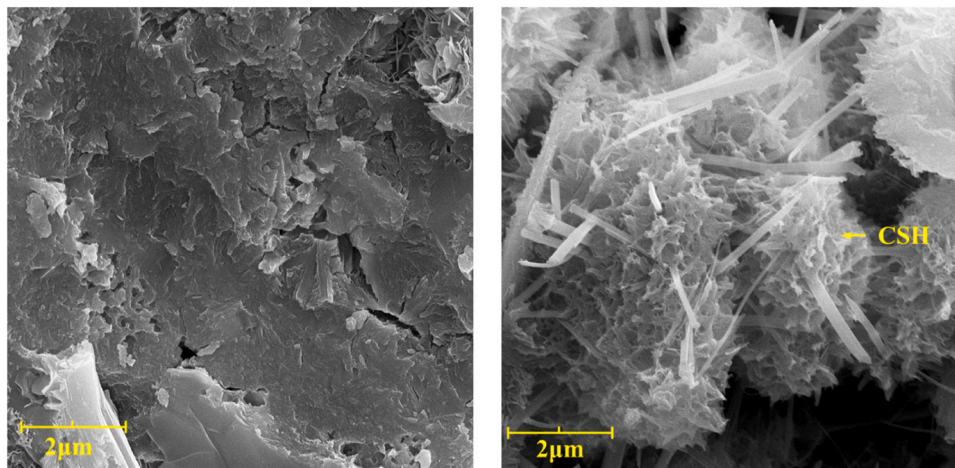


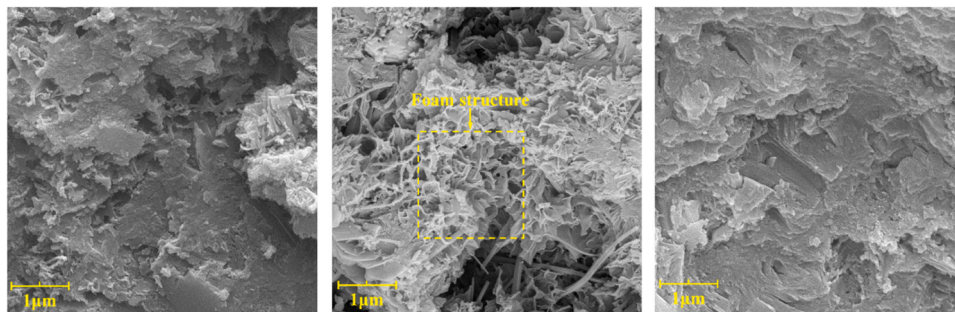
Fig. 12. Foam structure of CPI samples in vacuum (80000x).



(a) A28

(b) A3V28

Fig. 13. SEM images of CPII samples at 28d age (30000x).

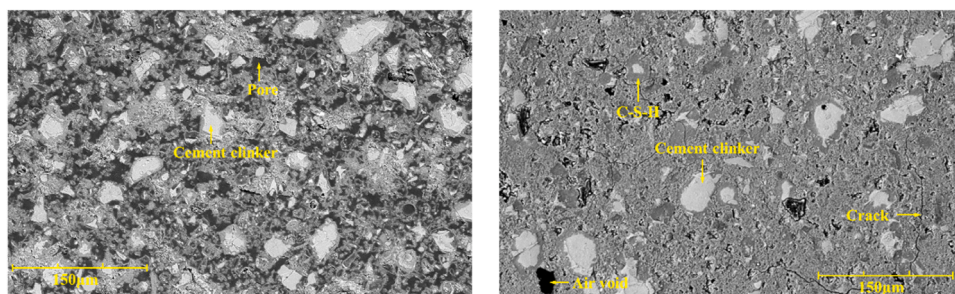


(a) A150

(b) A3V150

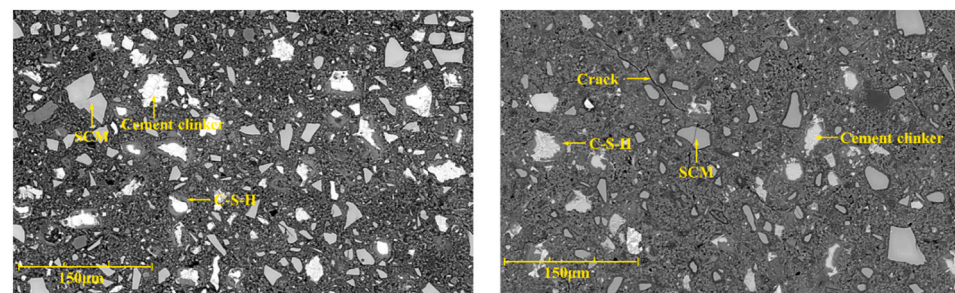
(c) A28V150

Fig. 14. SEM images of CPII samples at 150d age (30000x).



(a) CPI-A1V28

(b) CPI-A28



(c) CPII-A3V28

(d) CPII-A28

Fig. 15. BSE images of CPI and CPII samples.

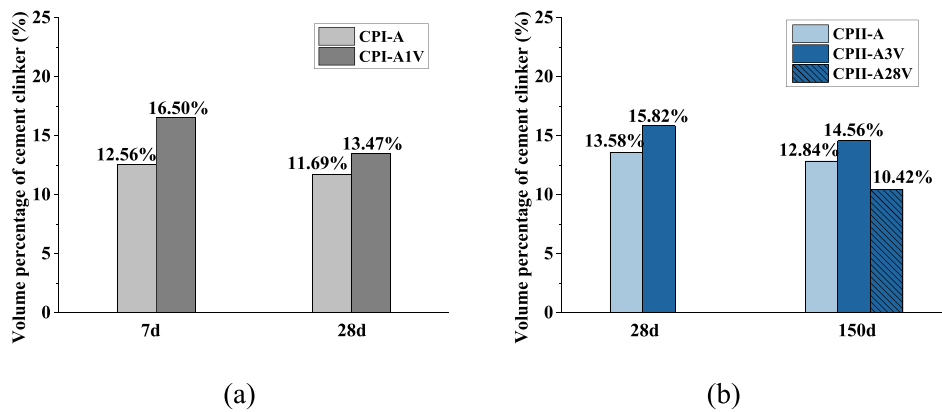


Fig. 16. Volume percentage of cement clinker in CPI and CPII samples.

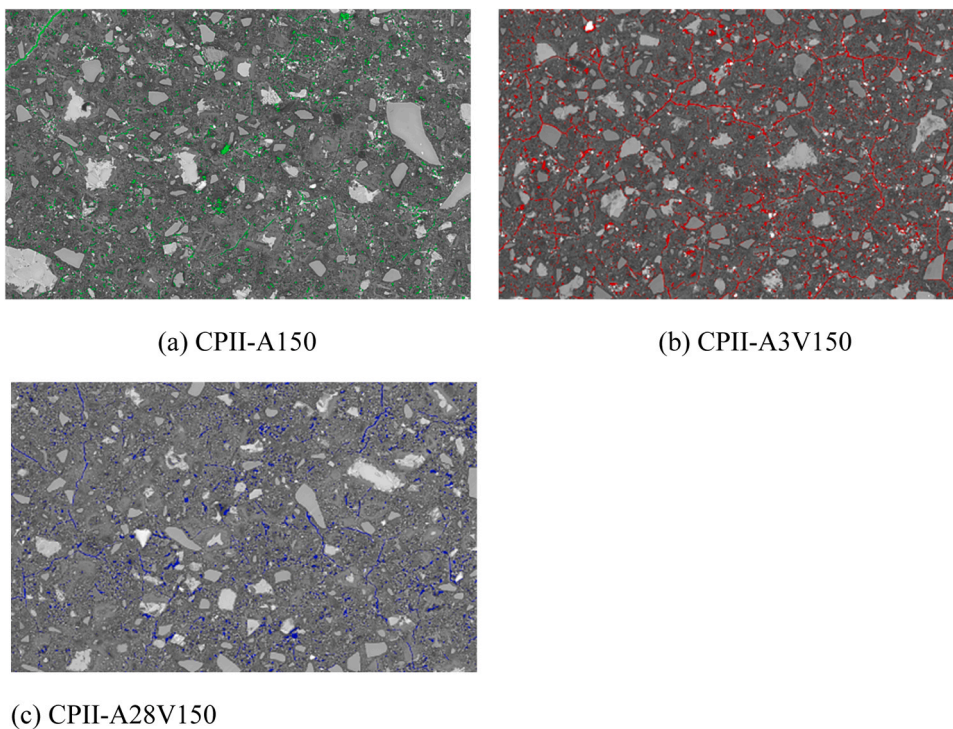


Fig. 17. Matrix cracking in CPII samples at 150 days age.

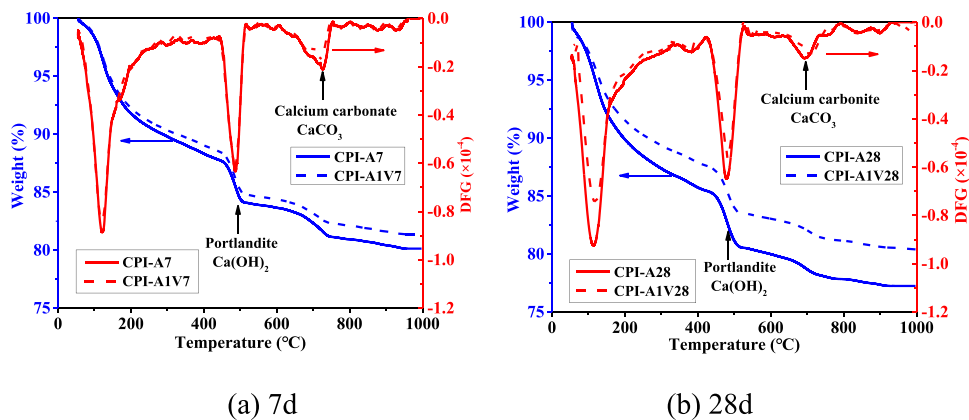


Fig. 18. TG-DTG curve of CPI samples.

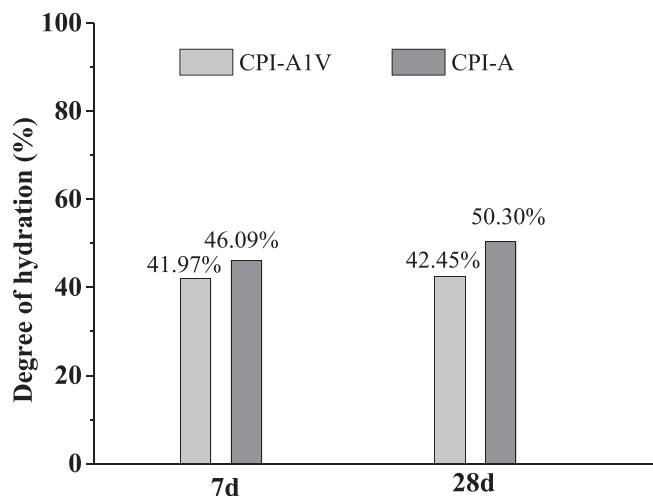


Fig. 19. Degree of hydration of CPI samples.

pore structure of cement stone. These conclusions are consistent with the findings in Section 3.2. This implies that the effects of vacuum exposure are more pronounced during the early stages of cement hydration, when the pore structure is still developing. However, as the cement continues to hydrate and harden, the pore structure becomes more stable and less susceptible to changes caused by vacuum exposure.

Fig. 23 shows the total porosity, mean pore diameter, and characteristic pore diameter of CPII specimens. The A3V specimens have significantly higher total porosity, mean pore diameter, and characteristic pore diameter than another two types of specimens. Meanwhile, the A28V specimens only exhibit a slight increase compared to atmospheric specimens, with a difference of less than 10%. It is also noteworthy that the total porosity of specimens in both environments decreases with age, while the mean pore diameter increases, which is the same with that observed in Fig. 21. This is due to the increasing amount of hydration products fill the free space previously occupied by free water, and results in a decrease in total porosity. Moreover, the C-S-H gels undergo continuous drying shrinkage, leading to the densification effect of the matrix, which reduces the gel pores between 3 and 12 nm [46], but gradually increases the interunit pores between 20 and 40 nm [50,51]. This phenomenon is more significant for specimens in vacuum environment, which undergo more significant shrinkage. Test data by Zhang et al. [45] also support this conclusion.

### 3.5. Development of drying shrinkage

Fig. 24 shows the shrinkage of C30 and C50 specimens. A clear influence of vacuum exposure on shrinkage can be observed. Once the specimens are moved to the vacuum tube, the development of shrinkage

is greatly accelerated. In vacuum environment, the development of shrinkage is stable, whereas atmospheric specimens exhibit significant fluctuations. This phenomenon is observed in both C30 and C50 concrete. It may be attributed to the susceptibility of specimens in the atmospheric environment to environmental factors such as air humidity, sunlight, rain, etc., as they are directly exposed to the outdoor environment without any protection.

For specimens exposed to vacuum, the shrinkage develops similarly, regardless of the type of concrete or the timing of vacuum exposure. The shrinkage rapidly increases and then gradually stabilizes after approximately 50–60 days of vacuum exposure. Compared to atmospheric specimens, specimens exposed to vacuum exhibit significantly greater shrinkage. At 280 days, the shrinkage of atmospheric specimens is around  $-280 \mu\epsilon$ , whereas C30SH-A28V specimens has a shrinkage of  $-465 \mu\epsilon$ , which is 66% larger. For C50 concrete, the increase is even more significant, at 300%. The latest study by Long et al. [25] also reported this phenomenon. The shrinkage of concrete is closely related to humidity, with lower relative humidity leading to larger shrinkage [52]. In vacuum, most of the free water inside the concrete evaporates, resulting in much lower relative humidity compared to normal conditions. Fig. 25 shows the relative humidity inside the concrete. The red curves represent the relative humidity, while the blue curves represent the temperature. Concrete in vacuum has significantly lower relative humidity than concrete in atmospheric environment. For instance, at 28 days and 90 days, the relative humidity of concrete in vacuum is 75% and 62%, respectively, while the corresponding values for atmospheric concrete are 95% and 76%. An interesting phenomenon observed is that the variation of relative humidity over time show similar trends with temperature. This has also been confirmed by Sekki et al. [53], who found that the internal relative humidity of concrete is temperature-dependent.

The shrinkage of C30 and C50 are compared in Fig. 26. In both environments, C30 and C50 concrete show similar shrinkage. In the early stage, the shrinkage of C50 concrete in the atmosphere is slightly larger than that of C30 concrete, however, the shrinkage of C30 concrete surpasses that of C50 concrete at the age around 60 d. This is because C50 concrete has more significant autogenous shrinkage at early ages due to a smaller water-cement ratio [54,55]. At later stages, C30 concrete shows more significant drying shrinkage due to a relative more porous internal structure. In vacuum, the total shrinkage of C30 concrete is close to that of C50 concrete.

### 3.6. Discussions

#### 3.6.1. Influence of vacuum exposure on hydration reaction

In the low-vacuum environment, the free water and air in the cement paste will quickly evaporate. As shown in Fig. 25, after only two weeks' vacuum exposure, the relative humidity in concrete drops to below 80%. The reduction in free water will directly reduce the amount of

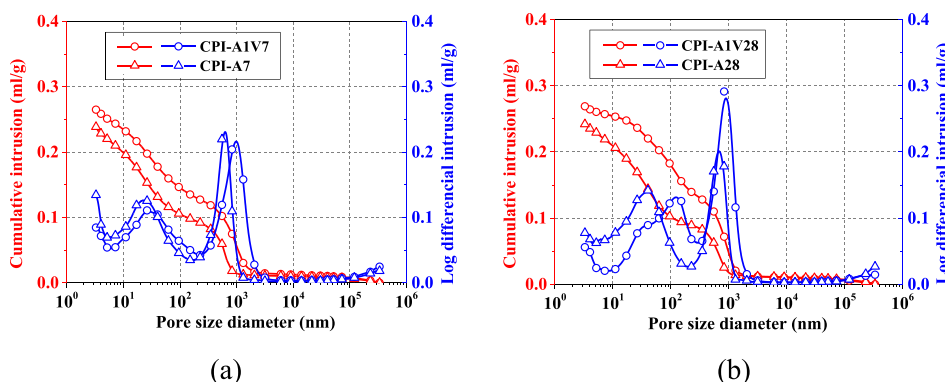


Fig. 20. Cumulative pore volume and pore size distributions of CPI specimens.

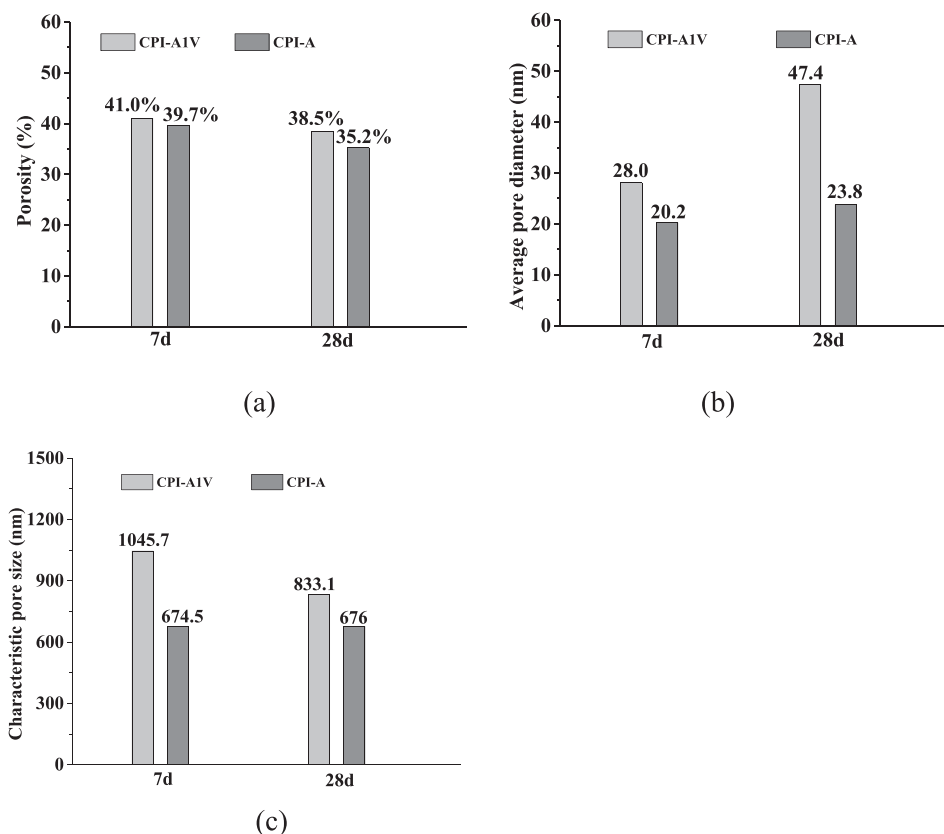


Fig. 21. Characteristic values of pore structure of CPI samples.

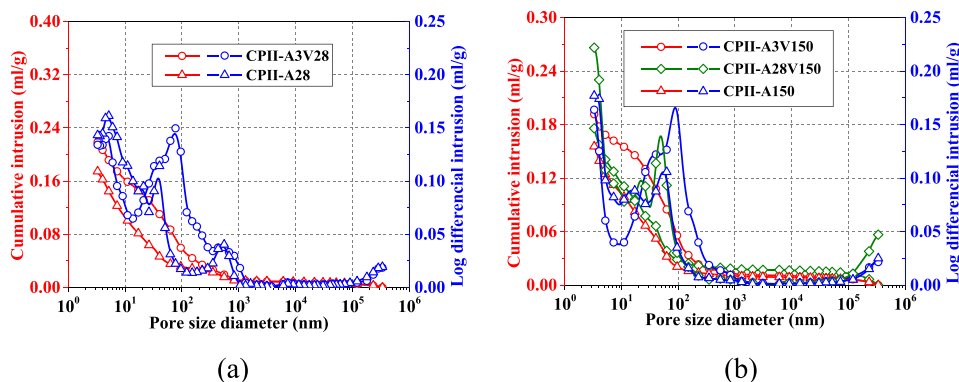


Fig. 22. Cumulative pore volume and pore size distributions of CPII specimens.

hydration products. Consequently, the original water-filled spaces cannot be filled with hydration products, and the volume of capillary pores will be increased. In addition, due to the reduction of water content, the diffusion coefficient of free water in the hardened paste decreases, and the cement hydration reaction will slow down or even stop. Studies have shown that when the relative humidity is below 80 %, the cement hydration reaction will stop [52,56]. Therefore, when concrete is subjected to vacuum at early ages, the amount of hydration products and the degree of hydration will be reduced. Results in Section 3.3 confirm this conclusion. Chen et al. [57] also observed that under the same relative humidity conditions, the chemical-bound water of cement paste cured in low pressure environment was less than that in normal conditions.

3.6.2. Influence of vacuum exposure on hydration products

In vacuum, the generated hydration products are inferior to those

generated in atmosphere. In the hardening of cement paste, the trapped air in the matrix diffuses to the outer environment with the volume expanding. This will result in the foam structure in the hydration products, as shown in Fig. 12. The poor quality of hydration products, particularly the C-S-H gels which are the main contributor of concrete strength, will certainly compromise the mechanical properties of concrete.

3.6.3. Influence of vacuum exposure on the mechanical properties

In vacuum, concrete loses a large amount of water, which leads to a decrease of the degree of hydration and hydration products, and an increase of matrix porosity. Previous studies by Shangguan et al. [24], Ge et al. [30] indicate that vacuum exposure also weakens the interface transition zone (ITZ) between cement and aggregates, which is caused by significant drying shrinkage and reduced cement hydration. All the above phenomenon are detrimental for mechanical properties.

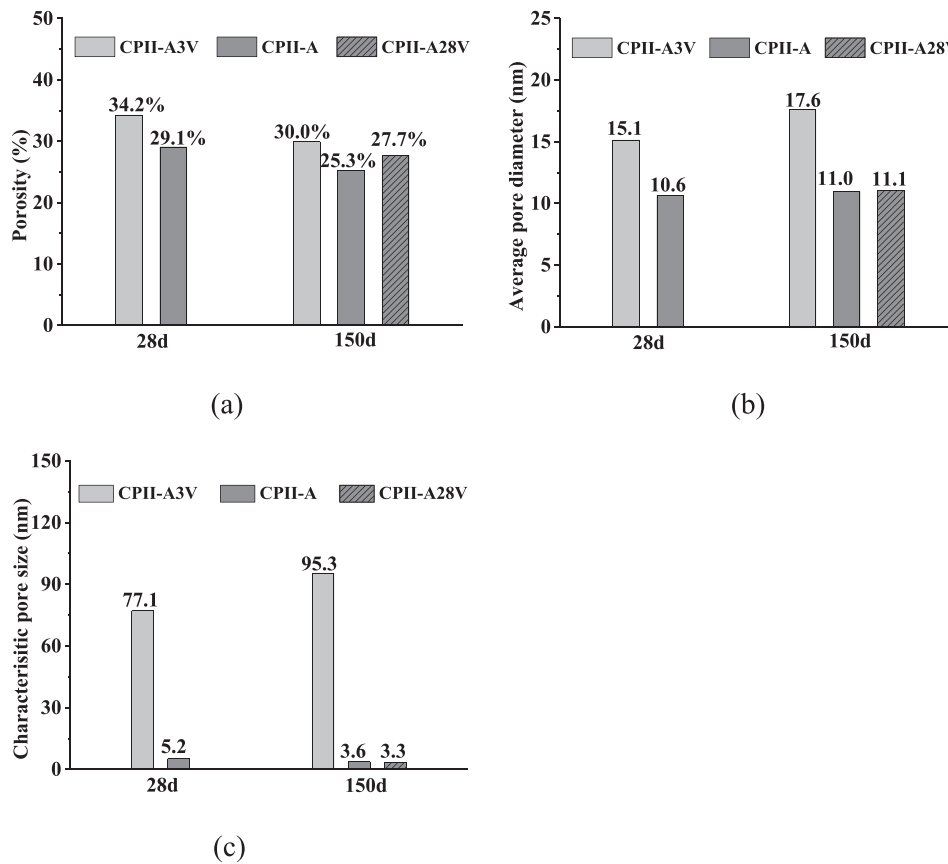


Fig. 23. Characteristic values of pore structure of CPII samples.

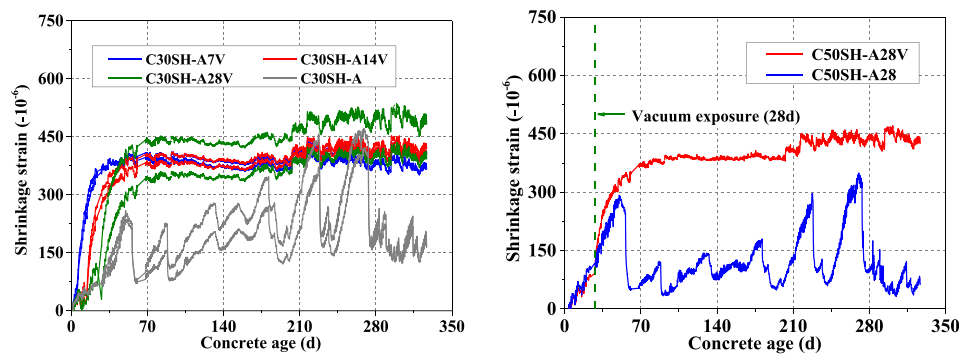


Fig. 24. Development of shrinkage of C30 and C50 concrete.

However, only concrete which is exposed to vacuum at early ages will show a significant decrease in mechanical properties. If the cement hydration reaction is almost completed at the time of vacuum exposure, the microstructure of concrete can hardly be affected, and the strength and elastic modulus will not decrease but may even increase, as described in Section 3.1.

In fact, vacuum exposure has both positive and negative effects on concrete, as shown in Fig. 27. On the one hand, vacuum exposure results in the closure of gel pores and the densification of matrix, thereby enhancing the mechanical properties. Similar phenomenon has been reported in previous studies [51,58,59]. On the other hand, vacuum exposure can coarsen concrete pores, and induce foam structure in C-S-H gels due to the rapid evaporation of water, which has a significant negative impact on the concrete matrix. In addition, the evaporation of free water also leads to insufficient water supply for the later-stage hydration of cement clinker, reducing the degree of cement hydration. The

combined effects of these factors significantly influence the concrete behavior.

When concrete is exposed to vacuum in the early ages, the free water in concrete will be significantly evaporated. Consequently, the hydration reaction is significantly inhibited, and bubble-like structures are generated in the hydration products. Since the C-S-H gels in the early ages have not yet started the transformation from low density structure to high density structure, the positive effects of vacuum exposure are not significant, and the negative effects of vacuum exposure are dominant in the early stage. When concrete is exposed to vacuum in the later stages of cement hydration, the microstructure of the cement paste has already formed, and the C-S-H gels have transformed from the low-density structure to the high-density structure. At this time, the low vacuum environment shows a strengthening effect on the matrix. Moreover, in the later stages of hydration reaction, the free water decreases, and the evaporation of free water is not significant. The cement hydration

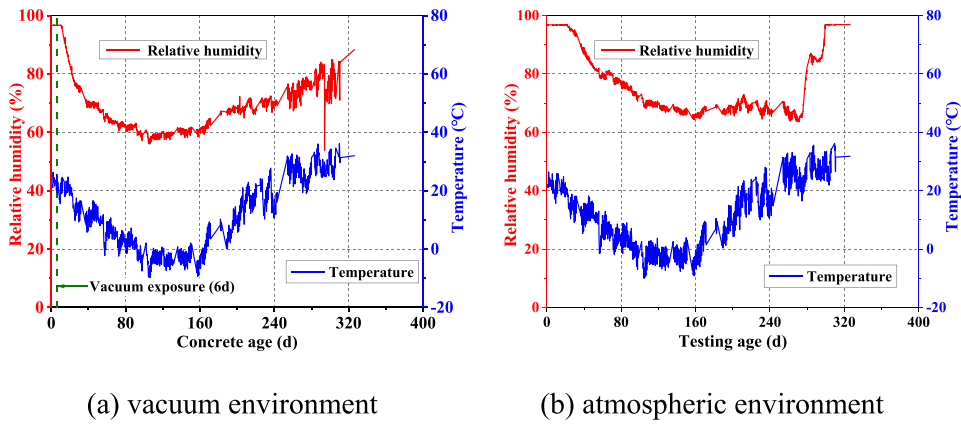


Fig. 25. Relative humidity and temperature of C30 concrete at different ages.

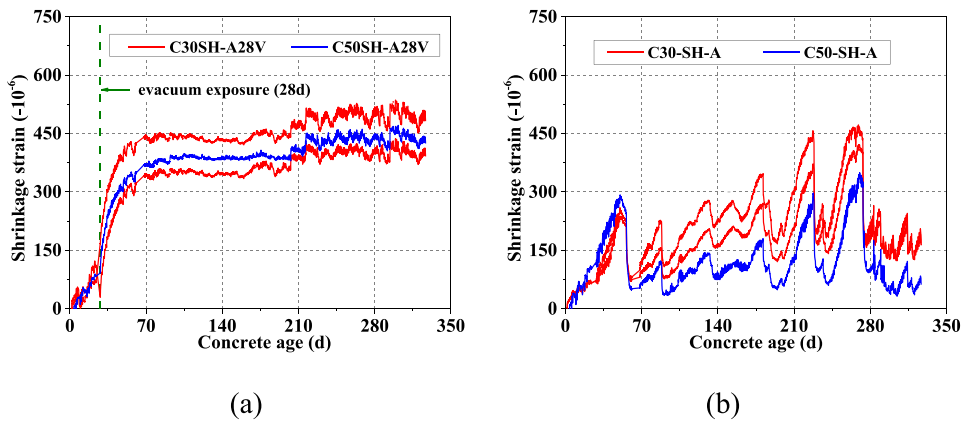


Fig. 26. Comparisons of shrinkage between C30 and C50 concrete.

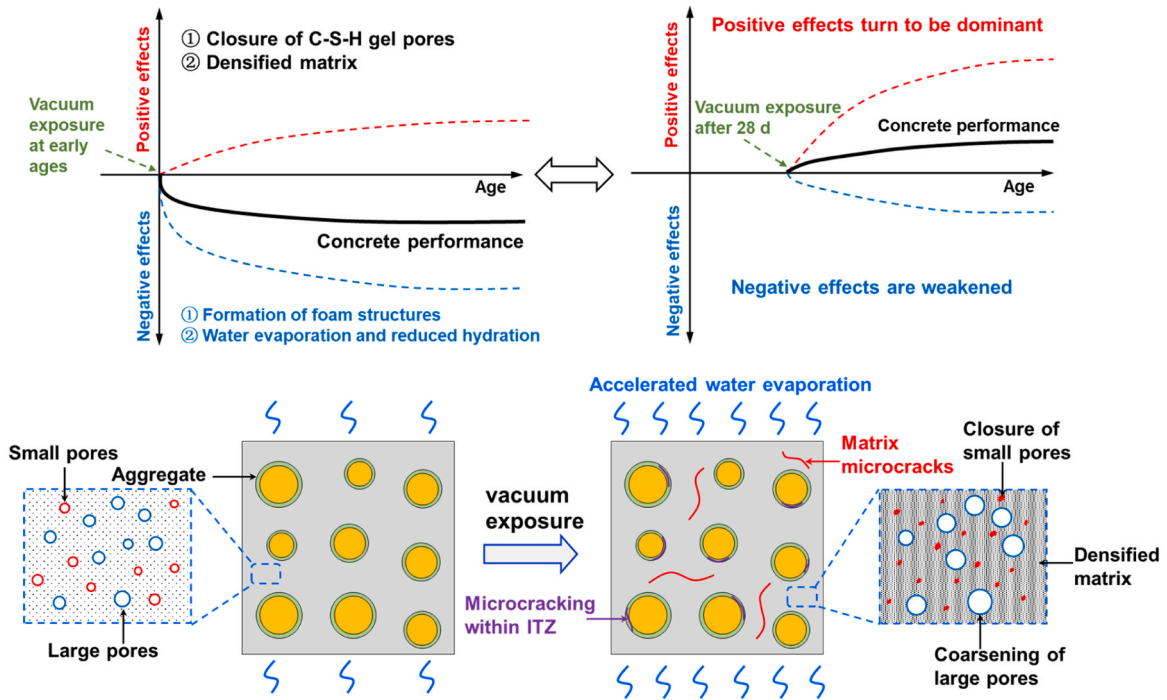


Fig. 27. Mechanism of effects of vacuum exposure on concrete.

reaction gradually slows down, and the formation of bubble-like structures is less likely to occur. Therefore, the negative effects of vacuum exposure are significantly suppressed. Hence, vacuum exposure during the later stage of cement hydration shows positive effects on concrete.

#### 4. Conclusions

This paper provides a deep insight into the effects of vacuum exposure on the concrete behavior. Based on the results and discussions above, the following conclusions can be drawn:

(1) Vacuum exposure of concrete at early ages is detrimental for concrete; however, if vacuum exposure is started when the cement hydration is stagnant, the mechanical properties of concrete can hardly be affected. In some cases, improvement of strength and elastic modulus can be observed due to densification of matrix.

(2) In the vacuum environment, the cement hydration is significantly impeded, and the reaction rate and degree of hydration are lower than those in normal environments. The hydration products are significantly reduced, and the micro-structure of the hydration products is deteriorated. The porosity and pore size of hardened cement paste are significantly increased.

(3) Compared with that in normal conditions, the C-S-H gels generated in vacuum environment is altered in morphology, which is characterized by a porous foam-like structure. The foam structure has a large number of pores below 1  $\mu\text{m}$ , and it will not disappear with increase of concrete age.

(4) Vacuum exposure at both early and later ages of concrete show similar effects on C30 concrete and C50 concrete. However, compared with C30 concrete, C50 concrete is less affected by the negative effects of vacuum exposure.

(5) In the low vacuum environment, the relative humidity inside the concrete decreases rapidly, resulting in the rapid development of shrinkage of concrete. Compared to concrete in atmosphere, the shrinkage of concrete in vacuum is significantly increased.

(6) For concrete subjected to vacuum exposure at different ages, the development of shrinkage follows a similar pattern, with little difference in the total shrinkage. The earlier the vacuum exposure initiates, the earlier the shrinkage strain converges.

#### CRedit authorship contribution statement

**Yalin Liu:** Methodology, Investigation. **Peng Feng:** Supervision, Conceptualization. **Guanzhi Cheng:** Validation, Resources. **Siming Liang:** Writing – review & editing, Methodology. **Bing Han:** Supervision, Funding acquisition. **Haosu Liu:** Resources, Methodology, Funding acquisition. **Hailong Ye:** Writing – review & editing. **Hongwei Lin:** Writing – original draft, Investigation, Funding acquisition, Formal analysis. **Song Han:** Writing – review & editing, Methodology, Investigation.

#### Declaration of Competing Interest

The authors declare that they have no known competing financial interests or personal relationships that could have appeared to influence the work reported in this paper.

#### Data Availability

Data will be made available on request.

#### Acknowledgements

The authors would like to acknowledge the Institute of Magnetic Levitation and Electromagnetic Propulsion, China Aerospace Science and Industry Corporation Limited for technical collaborations and funding this work. This work is also funded by the National Natural

Science Foundation of China (No. 51978379), and Research Programs of CARS (2022YJ129). The first author also wishes to thank master students Huixin Zeng, Ziqin Liu and Bingchuan Yan for their considerable help in fabricating and loading the concrete specimens.

#### References

- [1] H. Bi, B. Lei, 2009, Aerodynamic characteristics of evacuated tube high-speed train. In: second international conference on transportation engineering. Chengdu, China, 2009..
- [2] F. Lluésma, A. Arguedas, S. Hoyas, A. Sánchez, J. Vicén, Evacuated-tube, high-speed, autonomous maglev (hyperloop) transport system for long-distance travel: an overview, *IEEE Electron. Mag.* 9 (4) (2021) 67–73.
- [3] E. Musk, Hyperloop alpha. White Paper, CA, USA (2013).
- [4] P. Devkota, H.W. Jang, J. Hong, J. Park, Finite element analysis-based damage metric for airtightness performance evaluation of concrete tube structures, *KSCSE J. Civ. Eng.* 25 (4) (2021) 1385–1398.
- [5] Z. Liu, S. Stichel, M. Berg, Overview of technology and development of maglev and hyperloop systems, *KTH R. Inst. Technol., Stockh., Swed.* (2022).
- [6] J. Lim, C. Lee, Y.J. Oh, J. Jo, J. Lee, K. Lee, et al., Equivalent inductance model for the design analysis of electrodynamic suspension coils for hyperloop, *Sci. Rep.* 11 (1) (2021) 23499.
- [7] B. Han, L. Liu, K. Wang, J. Zhang, T. Zhou, Z. Su, 2021, Performance analysis of train-ground communication system for vacuum tube high-speed flying train. In: 7th international conference on computer and communications. Chengdu, China, 2021.
- [8] A. Santangelo, The infrastructure challenges of hyperloop, *Procedia Struct. Integr.* 44 (2023) 626–632.
- [9] D. Braak, Concrete hyperloop: a feasibility study on the application of concrete tubes in the hyperloop infrastructure, Master Thesis, Delft Univ. Technol., Neth. (2019).
- [10] T.D. Lin, Concrete for lunar base construction, : lunar bases Space Act. 21st Century Houst., US (1985).
- [11] M.Z. Naser, A.I. Chehab, Materials and design concepts for space-resilient structures, *Prog. Aeosp Sci.* 98 (2018) 74–90.
- [12] Z. Hu, T. Shi, M. Cen, J. Wang, X. Zhao, C. Zeng, et al., Research progress on lunar and martian concrete, *Constr. Build. Mater.* 343 (2022) 128117.
- [13] Cullingford H.S., Keller M.D. In: 2nd conference on lunar bases and space activities. Houston, USA, 1992.
- [14] H.S. Cullingford, M.D. Keller, R.W. Higgins, Compressive strength and outgassing characteristics of concrete for large vacuum-system construction, *J. Vac. Sci. Technol.* 20 (4) (1982) 1043–1047.
- [15] L.J. Powers-Couche, T.D. Lin, 1996, Behavior of fresh mortar in a vacuum and microstructure of mortar hardened in a vacuum. In: 5th International Conference on Space. New Mexico, USA, 1996.
- [16] T. Horiguchi, N. Saeki, T. Yoneda, T. Hoshi, T.D. Lin, Behavior of simulated lunar cement mortar in vacuum environment, : 6th ASCE Spec. Conf. Expo. Eng., Constr., Oper. Space (1998).
- [17] Y. Sakoi, T. Horiguchi, N. Saeki, Durability of hardened mortar under high-vacuum condition. Cement Combinations for Durable Concrete, Proceedings of the international conference held at the University of Dundee, Scotland, UK, 2005.
- [18] N. Hatanaka, T. Ishida, Hydration reaction and strength development of lunar concrete under vacuum condition, *SAE Trans.* 113 (2004) 324–334.
- [19] Hatanaka N., Perino M.A. Lunar concrete radiation shielding production for primary lunar base: SAE Technical Paper, 2007.
- [20] H. Kanamori, S. Matsumoto, N. Ishikawad, Long-term properties of mortar exposed to a vacuum, *Acids Spec. Publ.* 125 (1991) 57–70.
- [21] H. Namba, N. Ishikawa, H. Kanamori, T. Okada, 1988, Concrete production method for construction of lunar bases. In: engineering, construction, and operations in space, proceedings of the ASCE. New York, USA, 1988.
- [22] S. Pilehvar, M. Arnhof, A. Erichsen, L. Valentini, A.L. Kjøniksen, Investigation of severe lunar environmental conditions on the physical and mechanical properties of lunar regolith geopolymers, *J. Mater. Res Technol.* 11 (2021) 1506–1516.
- [23] H. Chang, X. Wang, Y. Wang, S. Li, J. Wang, J. Liu, et al., Influence of low vacuum condition on mechanical performance and microstructure of hardened cement paste at early age, *Constr. Build. Mater.* 346 (2022) 128358.
- [24] M. Shangquan, Y. Xie, S. Xu, C. Gao, G. Long, F. Wang, et al., Mechanical properties characteristics of high strength concrete exposed to low vacuum environment, *J. Build. Eng.* 63 (2023) 105438.
- [25] G. Long, Y. Chen, Z. Tang, M. Shangquan, C. Gao, S. Xu, Drying shrinkage behavior of cement mortar under low vacuum conditions, *Constr. Build. Mater.* 374 (2023) 130933.
- [26] X. Li, Z. Fu, Z. Luo, Effect of atmospheric pressure on air content and air void parameters of concrete, *Mag. Concr. Res* 67 (8) (2015) 391–400.
- [27] Y. Li, Z. Wang, L. Wang, The influence of atmospheric pressure on air content and pore structure of air-entrained concrete, *J. Wuhan. Univ. Technol. Mater. Sci. Ed.* 34 (2019) 1365–1370.
- [28] J. Huo, Z. Wang, H. Chen, R. He, Impacts of low atmospheric pressure on properties of cement concrete in plateau areas: a literature review, *Mater* 12 (9) (2019) 1384.
- [29] X. Ge, Y. Ge, Y. Du, X. Cai, Effect of low air pressure on mechanical properties and shrinkage of concrete, *Mag. Concr. Res* 70 (18) (2018) 919–927.
- [30] X. Ge, Y. Ge, Q. Li, X. Cai, W. Yang, Y. Du, Effect of low air pressure on the durability of concrete, *Constr. Build. Mater.* 187 (2018) 830–838.

- [31] R. He, Z. Yang, V.J. Gan, H. Chen, D. Cao, Mechanism of nano-silica to enhance the robustness and durability of concrete in low air pressure for sustainable civil infrastructures, *J. Clean. Prod.* 321 (2021) 128783.
- [32] X. Zeng, X. Lan, H. Zhu, G. Long, Y. Xie, Investigation on air-voids structure and compressive strength of concrete at low atmospheric pressure, *Cem. Concr. Compos* 122 (2021) 104139.
- [33] X. Chen, X. Liu, B. Tian, Y. Ge, L. Li, Effect of low atmospheric pressure on air entrainment in cement-based materials: an on-site experimental study at different elevations, *Mater* 13 (18) (2020) 3975.
- [34] Z. Liu, B. Lou, A. Sha, P. Du, X. Wang, Microstructure characterization of portland cement pastes influenced by lower curing pressures, *Constr. Build. Mater.* 227 (2019) 116636.
- [35] GB 175-2007, *Common Portland Cement*, CN, 2007.
- [36] GB/T 50081-2019, *Standard for test methods of concrete physical and mechanical properties*, CN, 2019.
- [37] A. Das, L. Reiter, R.J. Flatt, Early-age hydration mechanism of ternary binders: quantitative relation between microstructure evolution and strength build-up, *Cem. Concr. Res.* 170 (2023) 107191.
- [38] S. Liang, H. Du, Z. Ke, Y. Wei, J. Liu, Nonlinear creep of early-age cement mortar assessed by minutes-long flexural test, *Constr. Build. Mater.* 358 (2022) 129442.
- [39] S. Liang, Y. Wei, X. Gao, Strain-rate sensitivity of cement paste by microindentation continuous stiffness measurement: implication to isotache approach for creep modeling, *Cem. Concr. Res.* 100 (2017) 84–95.
- [40] C.J. Shi, Q. Yuan, *Analyzing method of cementitious materials*, Beijing: China Architecture & Building Press, 2018.
- [41] S. Han, Y.Q. Tu, M.Z. An, Z.R. Yu, The shrinkage of reactive powder concrete in early age and its control methods, *China Railw. Sci.* 36 (2015) 40–47.
- [42] Q.Q. Zhang, Y. Wei, Quantitative analysis on reaction degree of slag-cement composite system based on Back-Scattered-Electron image, *J. Chin. Ceram. Soc.* 43 (2015) 563–569.
- [43] V. Kocaba, E. Gallucci, K.L. Scrivener, Methods for determination of degree of reaction of slag in blended cement pastes, *Cem. Concr. Res.* 42 (3) (2012) 511–525.
- [44] H.W. Lin, S. Han, Effects of alternating air pressure cycles on the internal structure of concrete. Technical report. Beijing: Beijing Jiaotong University, 2023.
- [45] L. Zhang, X. Qian, C. Yu, M. Fang, K. Qian, J. Lai, Influence of evaporation rate on pore size distribution, water loss, and early-age drying shrinkage of cement paste after the initial setting, *Constr. Build. Mater.* 226 (2019) 299–306.
- [46] J. Yin, W. Li, J. Wang, X. Kong, Irreversible microstructural changes of calcium silicate hydrate during the first drying-resaturation cycle, *Cem. Concr. Res.* 163 (2023) 107032.
- [47] M.C. Alonso, J. Vera-Agullo, L. Guerreiro, V. Flor-Laguna, M. Sanchez, M. Collares-Pereira, Calcium aluminate based cement for concrete to be used as thermal energy storage in solar thermal electricity plants, *Cem. Concr. Res.* 82 (2016) 74–86.
- [48] I. Janotka, A. Ray, S.C. Mojumdar, The hydration phase and pore structure formation in the blends of sulfoaluminate-belite cement with portland cement, *Cem. Concr. Res.* 33 (4) (2003) 489–497.
- [49] T. Perraki, E. Kontori, S. Tsivilis, G. Kakali, The effect of zeolite on the properties and hydration of blended cements, *Cem. Concr. Compos* 32 (2) (2010) 128–133.
- [50] S. Han, D. Liu, G. Zhang, M.Z. An, Mechanism of curing effect on pore structure of hardened cementitious composites with ultra-low water to binder ratio, *J. Chin. Soc.* 45 (11) (2017) 1594–1604.
- [51] S. Han, Y.F. Cui, Y.F. Zheng, M.Z. An, Z.R. Yu, Mechanical properties and pore-structure of hardened cement paste with low water-binder ratio, *J. Chin. Soc.* 47 (2) (2019) 153–160.
- [52] S. Liang, Y. Wei, Methodology of obtaining intrinsic creep property of concrete by flexural deflection test, *Cem. Concr. Compos* 97 (2019) 288–299.
- [53] P. Sekki, P. Huttunen, T. Karvinen, J. Vinha, Temperature dependence of concrete drying and a method for estimating the effect of temperature on the relative humidity in concrete pores, *J. Build. Eng.* 89 (2024) 109266.
- [54] E. Tazawa, S. Miyazawa, Influence of cement and admixture on autogenous shrinkage of cement paste, *Cem. Concr. Res.* 25 (2) (1995) 281–287.
- [55] M. Yio, M.J. Mac, Y.X. Yeow, H.S. Wong, N.R. Buenfeld, Effect of autogenous shrinkage on microcracking and mass transport properties of concrete containing supplementary cementitious materials, *Cem. Concr. Res.* 150 (2021) 106611.
- [56] R.G. Patel, D.C. Killoh, L.J. Parrott, W.A. Gutteridge, Influence of curing at different relative humidities upon compound reactions and porosity in portland cement paste, *Mater. Struct.* 21 (1988) 192–197.
- [57] X. Chen, X. Liu, S.H. Dong, Y. Ge, Cement hydration and pore structure development in low air pressure and low humidity, *J. Xi' Univ. Arch. Technol.* 53 (2021) 202–207.
- [58] J. Yang, S. Han, Q. Wang, et al., The influence of graphene oxide on the hydration and mechanical properties of cement-based materials with low water-binder ratio, *Cem. Concr. Compos* 152 (2024) 105640.
- [59] S. Han, D. Liu, G. Zhang, M. An, Z. Yu, Mechanism of curing effect on pore structure of hardened cementitious composites with ultra-low water to binder ratio, *J. Chin. Ceram. Soc.* 45 (11) (2017) 1594–1604.